

# RSC Advances



This is an *Accepted Manuscript*, which has been through the Royal Society of Chemistry peer review process and has been accepted for publication.

*Accepted Manuscripts* are published online shortly after acceptance, before technical editing, formatting and proof reading. Using this free service, authors can make their results available to the community, in citable form, before we publish the edited article. This *Accepted Manuscript* will be replaced by the edited, formatted and paginated article as soon as this is available.

You can find more information about *Accepted Manuscripts* in the [Information for Authors](#).

Please note that technical editing may introduce minor changes to the text and/or graphics, which may alter content. The journal's standard [Terms & Conditions](#) and the [Ethical guidelines](#) still apply. In no event shall the Royal Society of Chemistry be held responsible for any errors or omissions in this *Accepted Manuscript* or any consequences arising from the use of any information it contains.

Cite this: DOI: 10.1039/c0xx00000x

www.rsc.org/xxxxxx

ARTICLE TYPE

# Facile synthesis of polyaniline nanotubes and their enhanced stimuli-response under electric fields

Bomi Sim, Hyoung Jin Choi\*

Received (in XXX, XXX) Xth XXXXXXXXX 20XX, Accepted Xth XXXXXXXXX 20XX

DOI: 10.1039/b000000x

Polyaniline (PANI) nanotubes were fabricated successfully using a micelle soft-template method in the presence of oxalic acid as a dopant and applied as the dispersed phase of an electrorheological (ER) fluid. The obtained nanotubes were with averagely 110 nm in an external diameter and 10 nm in an internal diameter with several micrometers in length. The X-ray diffraction pattern confirmed the crystalline structure of PANI owing to its tubular morphology. The rheological characteristics of the flow curves and yield stress of its ER fluid when dispersed in silicone oil were examined using a rotational rheometer equipped with a high voltage generator. Under an electric field, the PANI nanotubes showed improved ER effects, confirming that elongated particles have enhanced ER properties due to the higher aspect ratio. The dielectric spectra also showed the relaxation time and polarizability of the PANI nanotube-based ER fluid, corresponding to its ER performance.

## 1. Introduction

Polyaniline (PANI) is one of the most well-known conducting polymers that has been widely studied due to its ease of synthesis, low cost, good chemical and thermal stability, sensitive response to an electric field, and reversible acid/base doping/dedoping process to control the conductivity.<sup>1,2</sup> Therefore, it has many engineering applications, including chemical sensors, anticorrosion coatings, electrodes, batteries, capacitors and so on.<sup>1</sup> As an electro-responsive polymer, PANI has been also studied extensively as a disperse phase of electrorheological (ER) fluids,<sup>2-4</sup> in which ER fluids generally consist of polarizable particles dispersed in an insulating liquid. ER fluids are often called smart materials because their structural and rheological phenomena observed in an electric field are reversible and tunable. When a high electric field is applied, ER fluids show a drastic increase in their shear viscosity as well as changes in rheological properties due to the formation of chain-like structures along the applied external electric field.<sup>5-7</sup> In the absence of an electric field, however, the fluids exhibit Newtonian-like behavior. In addition, it features electrically tunable viscoelasticity and precisely controllable rheological properties under various electric fields. Furthermore, the reversible, controllable and rapid response to an electric field gives ER fluids many applications, such as dampers, actuators, brakes, shock absorbers, engine mounts, clutches, haptic devices etc.<sup>8-10</sup>

To promote the potential applications of ER technology, a range of substances, such as high dielectric inorganics and

organics, conducting polymers, and their composites, have been developed for ER materials.<sup>4,11</sup> Nevertheless, the application of ER fluids based on PANI is still limited by either particle sedimentation or low yield stress. To overcome these weaknesses, various efforts have been made to enhance the yield stress including the fabrication of PANI/clay nanocomposites.<sup>12</sup>

On the other hand, the shape of particles is also considered as an important factor for ER properties. For example, in the case of a PANI-based ER fluid, the morphology of the PANI micro/nanostructures strongly influences the electronic/ionic properties.<sup>13</sup> Many studies have examined the electrorheology of nanofiber suspensions.<sup>14,15</sup> Compared to spherical particles, fibrous-shaped particles have been reported to exhibit a larger yield stress and induced dipole moments as well as lower rates of sedimentation not only in ER fluids, but also in magneto-responsive magnetorheological fluids.<sup>16-18</sup> Lee et al.<sup>19</sup> and Yin et al.<sup>20</sup> reported that PANI tubes and PANI fibers exhibited an enhanced ER effect and sedimentation ratio than granular PANI, respectively. Heat treatment of the PANI nanotubes at various temperatures was found to result in a stronger ER effect compared to the corresponding granular PANI.<sup>21</sup> Compared to nanorods and nanospheres, titania-coated silica nanotubes<sup>22</sup> and PANI-coated titanate nanotube<sup>4</sup> were also showed higher yield stress and ER properties. Therefore, shaped controlling can improve the ER properties of suspensions.

Among the various ways to synthesize shape-controlled PANI, the soft template technique is one of the most effective methods because of easy processing, high yield, no organic solvents and no agitation.<sup>23-25</sup> In this method, many reagents can be used to synthesize PANI nanotubes.<sup>19,23-27</sup> Compared to other

dicarboxylic acid dopants, the oxalic acid-doped PANI has a conducting emeraldine salt phase predominantly and high conductivity.<sup>24,28</sup> The particle conductivity is an important factor in the ER effects.<sup>29</sup>

In this paper, PANI nanotubes were synthesized using a micelle soft-template method in the presence of oxalic acid as a dopant and adopted the dispersed phase in ER fluids. The experimental results showed that the PANI nanotube-based ER fluids exhibited improved rheological properties under various electric fields compared to the conventionally fabricated PANI-based ER fluids.<sup>19</sup> The rheological and dielectric properties were measured, and their correlation was investigated further.

## 2. Experimental

### 2.1 Materials and sample preparation

Aniline (DC Chemical, Korea), oxalic acid (Sigma-Aldrich) and ammonium persulfate (APS) (Daejung Co. Ltd., Korea) were used as received. Distilled (di) water was used in all experimental processes.

First, 2 mmol of aniline monomer and 0.5 mmol of oxalic acid were dissolved in di-water (10 ml) under sonication for 30 min. After cooled down to 4 °C, an aqueous solution of APS (2 mmol in 5 ml di-water) was added to the reactor under vigorous stirring. The resulting mixture was left to stand for 12 h at 4 °C without any disturbance. The product was washed sequentially with di-water, methanol and diethyl ether.<sup>24</sup> The electrical conductivity of the obtained PANI was controlled by a dedoping process for its ER fluid application. Specifically, the PANI nanotubes dispersed in di-water were sonicated for 30 min, and the pH was then adjusted to 9.0 using a 1 M NaOH solution. The density of the obtained PANI nanotubes was measured to be 1.41 g/cm<sup>3</sup>, whereas the electrical conductivity was decreased from  $9.5 \times 10^{-4}$  to  $4.7 \times 10^{-10}$  S/cm *via* a dedoping process. The PANI nanotubes were shaken through a molecular sieve (100 μm) to separate the agglomerated particles. A 10 vol% ER fluid was prepared by dispersing the PANI nanotubes in silicone oil (density: 0.96 g/cm<sup>3</sup>, kinematic viscosity: 50 cS).

### 2.2 Characterization

The morphology and particle size of the synthesized nanostructured PANI particles were characterized by both high resolution scanning electron microscopy (HR-SEM) (SU-8010, Hitachi) and transmission electron microscopy (TEM) (Philips CM200). Their chemical and crystalline structures were analyzed by Fourier transform infrared spectroscopy (FT-IR, VERTEX 80v, Bruker) and powder X-ray diffraction (XRD, DMAX 2500, Rigaku) using Cu Kα<sub>1</sub> radiation ( $\lambda = 0.154$  nm), respectively. The nitrogen adsorption-desorption isotherm was obtained using a Quantachrome Nova 3000 BET specific surface area analyzer at 77 K. In addition, the specific surface area of the sample was calculated using the Brunauer-Emmett-Teller method and the pore size distributions were calculated from the adsorption plots using the Barrett-Joyner-Halenda (BJH) model. The rheological properties of the ER fluid were measured using a rotational rheometer (Physica MCR 300, Anton Paar) equipped with a high voltage power supply (HCN 7E-12 500, Fug) and using Couette-type sample loading geometry with a bob and cup (CC 17/E, gap distance between cup and bob: 0.71 mm) at room temperature.

The electrical conductivity of the PANI nanotubes was measured using a 4-pin probe resistivity meter (QPP, Loresta-GP, Mitsubishi Chem. Co.) and the optical microscopy (OM, Olympus BX51) was also used to examine the fibrillation phenomenon of the ER fluid. Furthermore, the dielectric properties of the ER fluid were measured using a LCR meter (Agilent HP 4284A) in a liquid cell over the frequency range, 20 - 10<sup>6</sup> Hz.

## 3. Results and discussion

The PANI nanostructures, particularly nanotubes, were fabricated by a micelle soft-template method in the presence of oxalic acid as a dopant.<sup>24</sup> Fig. 1 shows SEM images of the PANI nanostructure synthesized and then doped with oxalic acid. Doping PANI with oxalic acid resulted in the formation of fibers, which were found by TEM to be hollow tubed (Fig. 2). The outer and inner diameter of the nanotubes distribute in the range of 90 – 130 nm and 6 – 12 nm with their mean value about 110 nm and 10 nm, respectively. PANI nanotubes have lengths of up to several micrometers. The aspect ratio by SEM and TEM analysis was *ca.* > 9, average in 18.

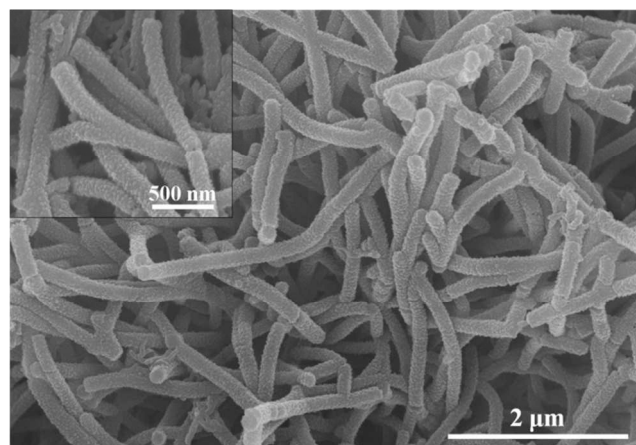


Fig. 1 SEM images of the PANI nanostructure. The inset is the SEM image under magnification.

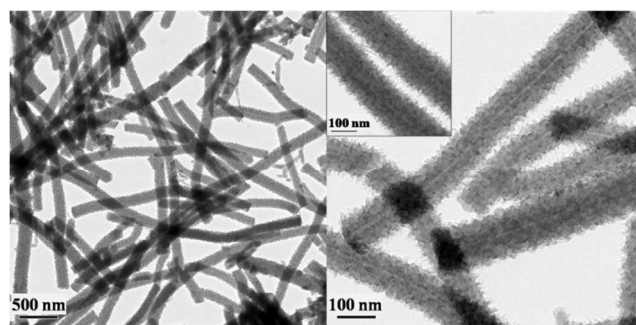


Fig. 2 TEM images of the PANI nanostructure. The inset is the TEM image under magnification.

Fig. S1 shows the FT-IR spectrum of the PANI nanotube. The characteristic bands of the emeraldine salt of the PANI were observed; the C=C stretching vibration of the quinoid and benzenoid rings at 1568 cm<sup>-1</sup> and 1492 cm<sup>-1</sup>, respectively.<sup>30</sup> In addition, the C-N stretching band of the secondary aromatic amine at 1303 cm<sup>-1</sup> and the N=Q=N absorption peaks (Q: the

quinoid ring) at  $1135\text{ cm}^{-1}$  were observed.<sup>14</sup> In particular, the absorption of the  $-\text{COOH}$  group at  $1041\text{ cm}^{-1}$  and  $509\text{ cm}^{-1}$  indicated that the resulting PANI had been doped with the carboxylic acid.<sup>23,24</sup>

Fig. S2 presents the XRD pattern of the synthesized PANI nanotubes. Peaks were observed at  $2\theta$  of  $6.4^\circ$ ,  $11.9^\circ$ ,  $18.9^\circ$ , and  $25.7^\circ$  and the corresponding inter-surface distances were  $13.8$ ,  $7.5$ ,  $4.7$ , and  $3.5\text{ \AA}$ , respectively. The peaks at  $18.9^\circ$  and  $25.7^\circ$  were assigned to the periodicity perpendicular and parallel to the polymer chain, respectively.<sup>31</sup> In particular, a sharp peak at  $6.4^\circ$  was attributed further to the separating aliphatic chains,<sup>32</sup> showing the orientation of the dicarboxylic acids in the polymeric chain, which was assigned as the periodic distance between the dopant and N atom on the adjacent main chains. These results confirm that the PANI nanotubes are of partly crystalline owing to their distinctive tubular morphology and possibly the presence of the double  $-\text{COOH}$  groups of the dicarboxylic acid.<sup>23</sup>

Isothermal adsorption-desorption curve and pore size distribution of the PANI nanotubes were obtained from the  $\text{N}_2$  adsorption measurements at  $77\text{ K}$ , as shown in Fig. S3. The BET surface area of the PANI nanotubes was  $57.8\text{ m}^2/\text{g}$ . This hysteresis loop exhibited a type IV isotherm. In addition, the mean pore size was approximately  $22.62\text{ nm}$  (Inset of Fig. S3).

Fig. 3 presents optical microscopy images of the distinctive characteristic ER phenomenon of the fibrillation process of PANI nanotubes dispersed in silicone oil under an applied electric field. Note that the ER fluids act as smart materials, whose rheological properties can be controlled precisely in an applied electric field.<sup>14,33,34</sup> Transformations in the microstructure of the ER fluid under an applied DC electric field using a DC high voltage source were observed by the OM. The gap distance between the parallel electrodes was fixed to  $150\text{ }\mu\text{m}$ . In the absence of an electric field, the particles were dispersed randomly in silicone oil like a Newtonian fluid. On the other hand, under an electric field ( $0.1\text{ kV}$ ) applied, the particles began to move and form rigid fibrillated chain structures in the direction of the electric field.

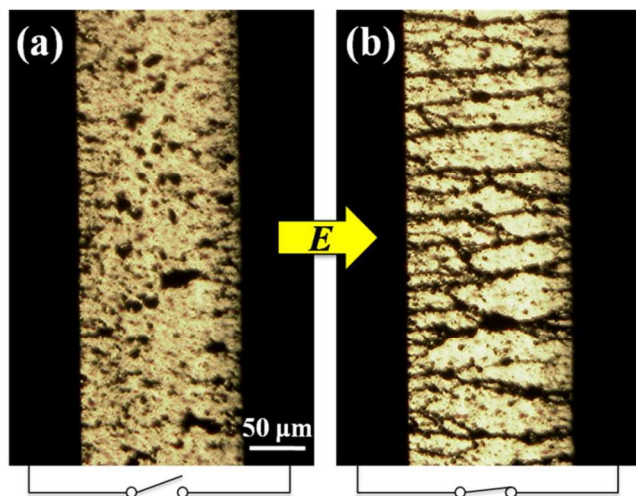


**Fig. 3** OM images of the PANI nanotubes-based ER fluid (10 vol%, 50 cS silicone oil) with and without an electrical field ( $0.1\text{ kV}$ ). A dilute ER fluid was dropped between two parallel electrodes ( $150\text{ }\mu\text{m}$ ) and observed by OM.

The flow curves of the PANI nanotubes suspension (10 vol%,

50 cS silicone oil) under the controlled shear rate (CSR) measurement mode was examined using a rotational rheometer equipped with a high voltage generator under a range of electric field strengths, as shown in Fig. 4(a). In the absence of an electric field, the shear stress increased linearly with increasing shear rate, in which the fluid behaved similar to a Newtonian fluid.<sup>35</sup> On the other hand, when a high electric field was applied, the ER fluid showed a large enhancement in shear stress because the particles were polarized and formed chain-like structures, as indicated in the OM images. When the strength of the electric field was enhanced, the shear stress of the PANI nanotube increased due to an inter-particle interaction force.<sup>37</sup> As a result of the chain-like structures, the ER fluid under an applied electric field is considered a Bingham fluid with yield stress, which is described as the shear stress extrapolated to the zero shear rate limit region.

When the ER properties were compared with those<sup>19</sup> of the previously studied PANI microtubes-based ER fluid, it was found that the PANI nanotube particle suspension exhibited higher shear stress than that of the PANI microtube under the same conditions, which agrees with the effect of the particle morphology on the ER properties investigated.<sup>20</sup> Anisotropic fibrous-like particles were reported to have the strongest ER effect than that of the spherical- and granular-shaped particle suspensions, which were attributed to the viscous drag force for a fibrous particle moving perpendicular to its long axis in a fluid that was significantly larger than a spherical particle of the same volume.<sup>37</sup> This results from the high aspect ratio, which makes particles link more strongly together and form robust chain structures.<sup>22,38</sup> For this reason, the PANI nanotubes show higher flow resistance and shear stress, which is induced when the fluid was sheared. Therefore, the aspect ratio presents an important role in improving the ER performance.<sup>16,17</sup> In the case of a particle suspension,<sup>39</sup> the particle with a high aspect ratio is well-known to have a larger viscosity than that with a smaller aspect ratio based on the increased drag coefficient related to the shape. This tendency explains that the increase in the aspect ratio of the PANI nanotube enhances the flow resistance owing to its high drag coefficient.

To examine the flow curves of an ER fluid, the simple Bingham fluid model is generally adopted, introducing the dynamic yield stress ( $\tau_y$ ) and shear viscosity ( $\eta$ ) of  $\tau_y = \tau + \eta\dot{\gamma}$ . The dynamic yield stress can be acquired by extrapolating the flow curve to a zero shear rate limit, but in the present case, there was an unusual decreasing trend in the shear stress in the high shear rate region. Therefore, in this study, a modified rheology equation of state, the Cho-Choi-Jhon (CCJ) model,<sup>40</sup> was used to describe the special shear stress behavior and yield stress.

$$\tau = \frac{\tau_0}{1 + (t_1\dot{\gamma})^\alpha} + \eta_\infty \left( 1 + \frac{1}{(t_2\dot{\gamma})^\beta} \right) \dot{\gamma} \quad (1)$$

The CCJ model, as shown in equation (1) was introduced to reanalyze the shear stress behavior by fitting the curves *via* six parameters. Here,  $\tau_0$  is a function of the electric field,  $t_1$  and  $t_2$  are the time constants used to describe the change in shear stress, and  $\eta_\infty$  is the shear viscosity at a high shear rate presented as the shear viscosity in the absence of an electric field. The exponent,  $\alpha$ , is related to the reduction in shear stress at the low shear rate region, whereas  $\beta$  in the range of 0 to 1.0 indicates the high shear rate region. Using the optimal parameters, the CCJ model showed a

much better fit to the flow curves than the Bingham model. The parameters are listed in Table 1.

Fig. 4(b) shows the shear viscosity as a function of the shear rate. Compared to the consistent viscosity at a zero electric field exhibiting Newtonian fluid characteristics, general shear thinning behavior was obtained under different electric field strengths.<sup>41</sup> The shear thinning behavior becomes increasingly significant with increasing shear rate and electric field strength.

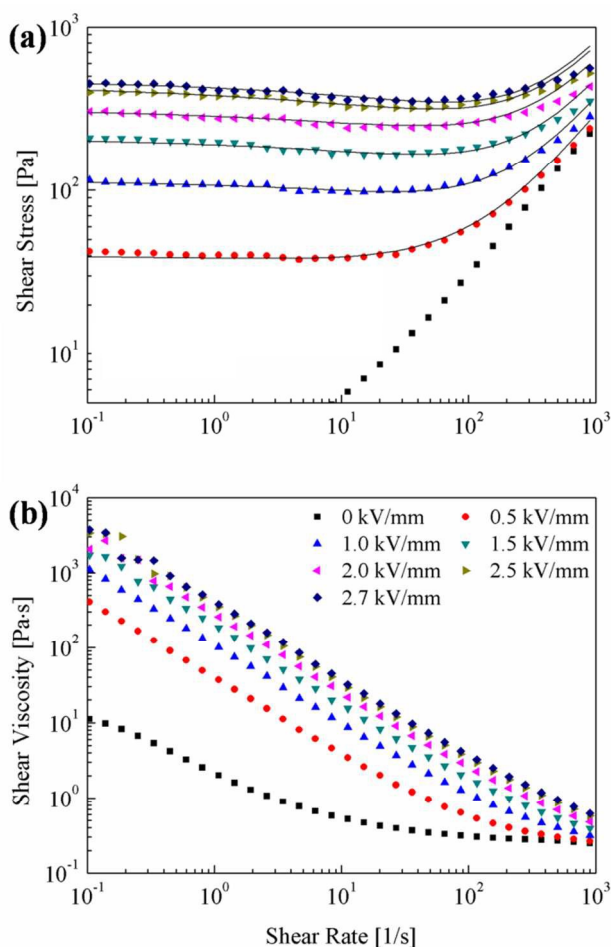


**Fig. 4** Flow curves of the PANI nanotubes-based ER fluid (10 vol%, 50 cS silicone oil) as a function of the shear rate with increasing electric field strengths. The line was fitted by the CCJ model.

**Table 1.** Fitting parameters in the CCJ model equation from the flow curves of PANI nanotubes-based ER fluid (10 vol%, 50 cS silicone oil).

Model Parameters	Electric field strength (kV/mm)					
	0.5	1.0	1.5	2.0	2.5	2.7
$\tau_{dy}$	39.95	113	207.59	319.61	446.67	452
$t_1$	0.0001	0.004	0.002	0.0015	0.003	0.005
$\alpha$	0.3	0.45	0.38	0.3	0.3	0.4
$\eta_\infty$	0.266	0.315	0.391	0.482	0.581	0.625
$t_2$	0.3	0.05	1	0.08	0.5	0.02
$\beta$	0.8	0.7	0.9	0.9	0.8	0.9

From the measured flow curves, the dynamic yield stresses ( $\tau_y$ ) were presented by extrapolating the shear stress at a  $0.1 \text{ s}^{-1}$  shear rate from Fig. 4(a). In general, the interrelationship between the dynamic yield stress and electric field strength ( $E$ ) can be

represented by a power-law relationship as follows:

$$\tau_y \propto E^\alpha \quad (2)$$

The power law index  $\alpha$  was suggested to be 1.5 in the conduction model, and  $\alpha = 2$  was indicated by the polarization model.<sup>42</sup> The power law dependence  $\alpha$  was found to approach 1.5 for these ER fluids (Fig. 5)

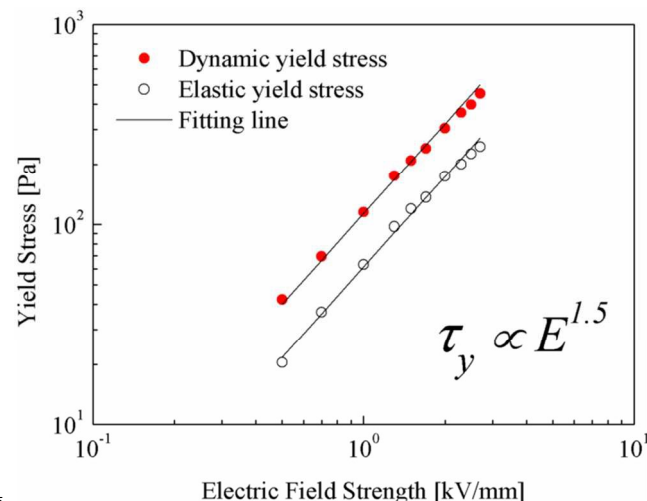


**Fig. 5** Yield stresses versus electric field strength for PANI nanotubes-based ER fluid (10 vol%, 50 cS silicone oil). The line is fitted by Eq. (2).

To examine the sensitivity and stability of the PANI nanotubes-based ER fluid, the shear stress was measured at a fixed shear rate of  $1 \text{ s}^{-1}$  using a square voltage pulse ( $t = 20 \text{ s}$ ), as shown in Fig. 6. Under each applied electric field, the shear stress increased upon the application of the external electric field and decreased immediately to a zero-field level when the electric field was removed. The transition of the shear stress at each turning point was fast and the shear stress was quite steady at the same electric field, indicating sensitive, reversible well-controlled ER characteristics. These are optimistic results for the applications of PANI nanotube-based ER materials in controlled mechanical systems.<sup>8-10,43</sup>

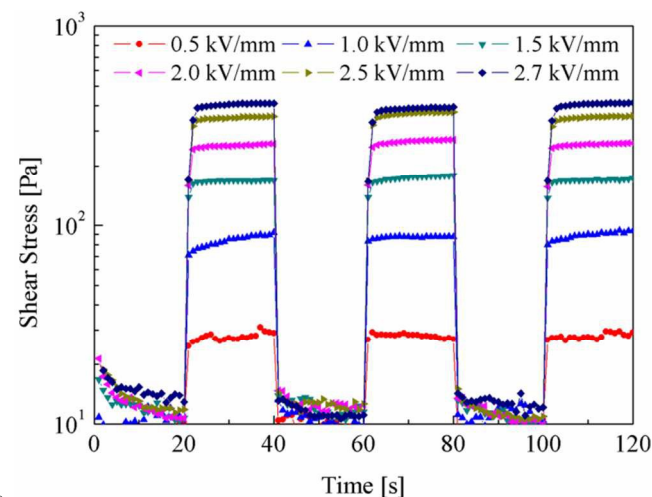


**Fig. 6** Shear stress of the PANI nanotubes-based ER fluid (10 vol%, 50 cS silicone oil) in the electric field with a square voltage pulse ( $t = 20 \text{ s}$ ) at a fixed shear rate of  $1 \text{ s}^{-1}$ .

A dynamic oscillation measurement was conducted to analyze the viscoelastic properties of the ER fluid. Before the test, the strain amplitude sweep tests were performed to find a linear viscoelastic region ( $\gamma_{LVE}$ ) at a certain angular frequency of 6.28 rad/s (1.0 Hz), as shown in Fig. 7(a). This specific angular frequency was recommended by the manufacturer and several previous experiments in ER systems were also performed at this frequency.<sup>16,44,45</sup> At the low strain region, the storage modulus,  $G'$ , is always higher than that of the loss modulus  $G''$ . In addition, the values of  $G'$  and  $G''$  are independent within the region of strain, which referred to as the linear viscoelastic region.<sup>46</sup> In the  $\gamma_{LVE}$ , the elasticity is superior ( $G' > G''$ ) compared to the viscosity, and the structures generated from the electric fields are the same. When the applied strain exceeds  $\gamma_{LVE}$ , both  $G'$  and  $G''$  are reduced significantly due to the irreversible transition in the structure of the ER fluid. In addition, the value of  $G''$  becomes larger than that of  $G'$ . This suggests that the structures begin to break down after a certain degree of deformation with the increased input strain. The elasticity of the ER fluid disappeared rapidly at a certain degree of strain.

Under the induced electric fields, the ER fluid showed a transition from a viscoelastic liquid to a viscoelastic solid.<sup>46</sup> This transition causes the formation of particle aggregates, string and then rigid column structures. In the strain amplitude sweep test, slight deformation results in an unstable state, as shown in Fig. 7(a). The data was reanalyzed to the magnitude of elastic component of stress ( $\tau' = G'\gamma$ ) as a function of strain, which is an effective way of examining the progressive structural breakdown,<sup>47</sup> (Fig. 7(b)). The rigidity of the fluid begins to deteriorate at the critical strain ( $\gamma_c$ ), which shows the linearity limit of the dynamic modulus.<sup>45</sup>  $\gamma_c$  increased linearly with increasing electric field from 0.08 to 0.2 %, as shown in the Fig. 7(b) inset. This yield strain point reflects the breaking of the interparticle bonds in the fluid network. This energy dissipation explains the decrease in  $G'$  and  $G''$  (Fig. 7(a)), as well as the sublinear strain-stress relationship in Fig. 7(b). With increasing electric field strength, the attraction force between the neighboring ER particles was enhanced, which tends to suppress bond breakage affecting the increase in  $\gamma_c$ . The elastic component of the stress increased linearly with strain within the linear viscoelastic limit, reaching equilibrium, after which yield or structural breakdown occurred. The maxima or shoulders of these points provide another way of examining the yield points.<sup>45,47</sup> The elastic yield stresses ( $\tau_c$ ) also increased with increasing applied electric field strength and showed a power-law dependence with an exponent of 1.5, as shown in Fig. 5. It is interesting to compare this result of  $\tau_c$  from dynamic oscillation test with the  $\tau_y$ , in which the dynamic yield stress  $\tau_y$  is obtained from the controlled shear rate measurement *via* an extrapolation method at a very low shear rate. On the other hand, it was further observed that the yield stress measured from the steady-state measurement is slightly larger than the one determined by dynamic investigation.<sup>48</sup> Nonetheless, both of the yield stresses as a function of electric field strength showed similar tendency.

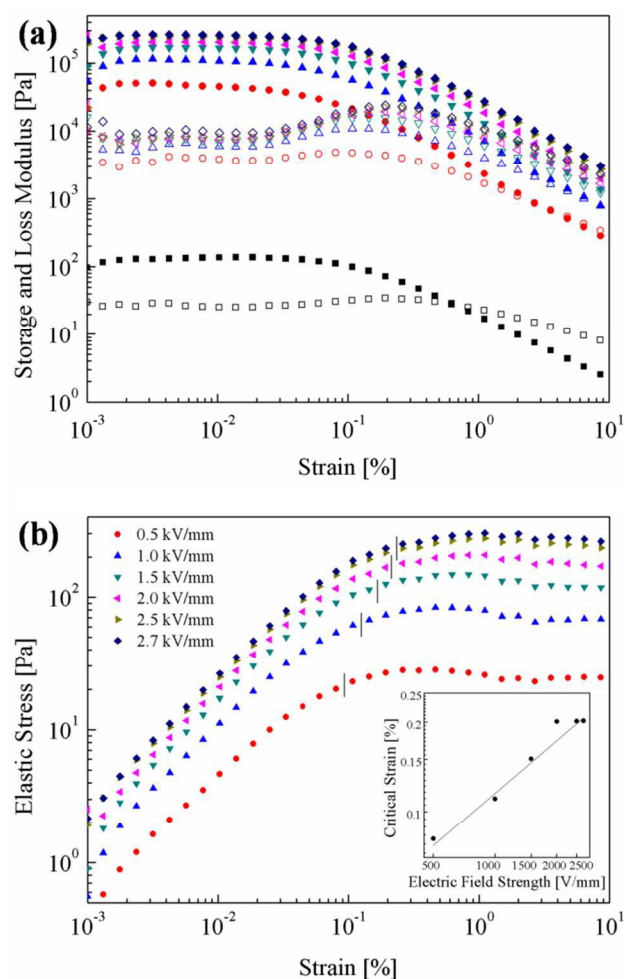


**Fig. 7** (a) Strain amplitude sweep ( $G'$ : closed,  $G''$ : open) and (b) elastic component of stress as a function of strain of the PANI nanotube-based ER fluid (10 vol%, 50 cS silicone oil). The vertical lines indicate the limit of linear viscoelasticity at each of electric field strength. The inset is a critical strain value.

Previously selected  $\gamma_{LVE}$  value was applied to the frequency sweep measurements. Both  $G'$  and  $G''$  were measured over the angular range, 1 to 100 rad/s, with a strain of 0.01 % in  $\gamma_{LVE}$ , as shown in Fig. 8(a). The  $G'$  and  $G''$  values increased with increasing electric field strength.  $G'$  was always higher than  $G''$ , suggesting the dominance of the elastic behavior beyond the viscous behavior in the structure of the ER fluid.  $G'$  was almost stable when the deformation frequency was increased to 100 Hz, which is similar to the typical behavior of combined colloidal dispersions and cross-linked rubber.<sup>49</sup> Moreover, the relaxation time for deformation was long enough and it is believed that the ER fluid with the interfacial polarized chain structures was not destroyed by deformation under the allowed condition. This increase in  $G'$  under an applied electric field indicates the enhanced solidification properties of the PANI nanotubes suspension.

This solid-like behavior can be explained by the damping factor,  $\tan \delta$ , which is defined as the ratio of the loss modulus (viscous) to the storage modulus (elastic) as follows:<sup>50</sup>

$$\tan \delta = G''(\omega)/G'(\omega) \quad (3)$$

Fig. 8(b) shows the  $\tan \delta$  value of the PANI nanotube as a function of angular frequency.  $\tan \delta$  was less than 1 over the entire frequency range representing solid-like properties of the PANI nanotube due to highly concentrated particulates. An increased electric field resulted in a decrease in  $\tan \delta$ , indicating that the strong particle interaction in the PANI nanotube and the elastic properties of PANI nanotube suspension were further enhanced compared to the lower electric field.

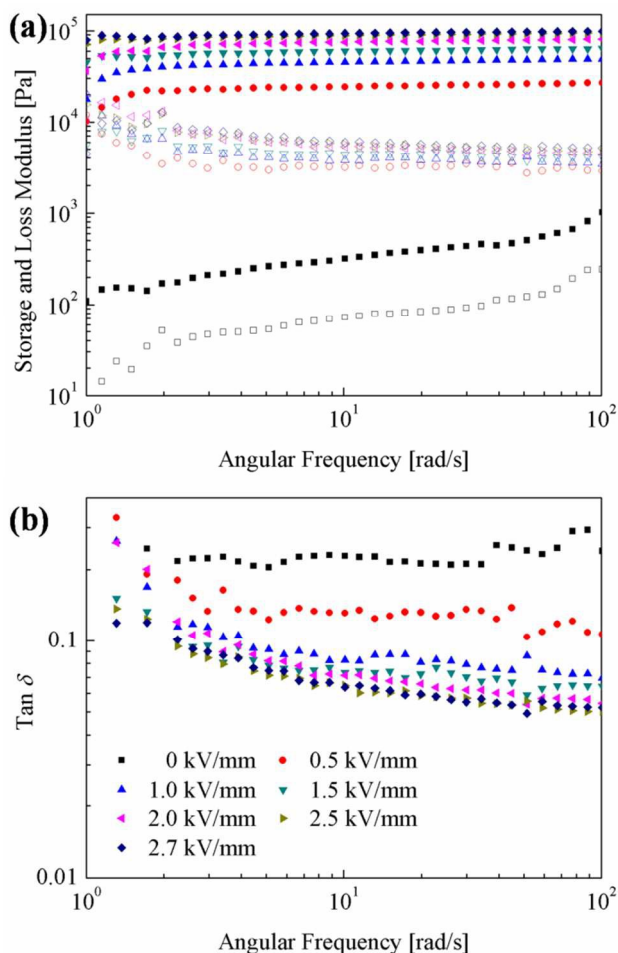


Fig. 8 (a) Frequency sweep ( $G'$ : closed,  $G''$ : open) and (b)  $\tan \delta$  curves of the PANI nanotube-based ER fluid (10 vol%, 50 cS silicone oil) as a function of angular frequency from an oscillatory shear test.

This change in PANI nanotubes to a solid-like state can also be confirmed by examining the stress relaxation behavior. Observing the relaxation behavior is one way of confirming the phase change in an ER fluid from a liquid-like to solid-like phase. Instead of performing the stress relaxation measurement directly, they can be estimated from the dynamic modulus data. Fig. 9 shows the stress relaxation behavior, in which the stress relaxation modulus  $G(t)$  was calculated from the values of  $G'(\omega)$  and  $G''(\omega)$  in Fig. 8(a) using the Schwarzl equation, which is the numerical formula given as follows:<sup>51,52</sup>

$$G(t) \cong G'(\omega) - 0.560G''(\omega/2) + 0.200G''(\omega) \quad (4)$$

The very short-term behavior of the material, which is difficult to obtain experimentally because of the intrinsic properties of polymeric materials and the limitation of the mechanical

measurement arising from the equipment itself, can be predicted from this equation.  $G(t)$  becomes linear with increasing electric field on a log-log scale, indicating that all are solid-like except in the absence of an electric field.

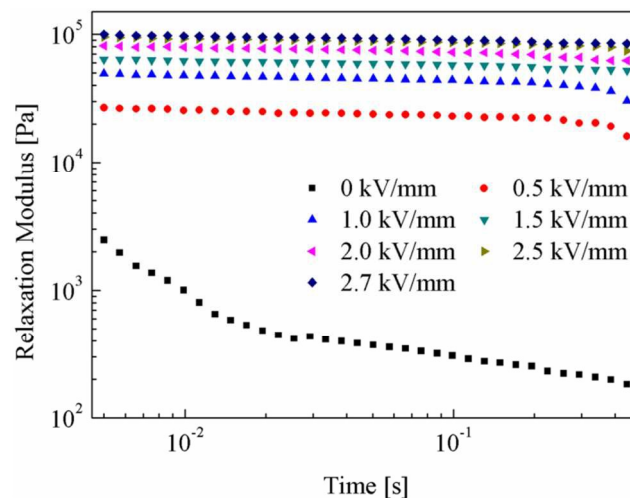
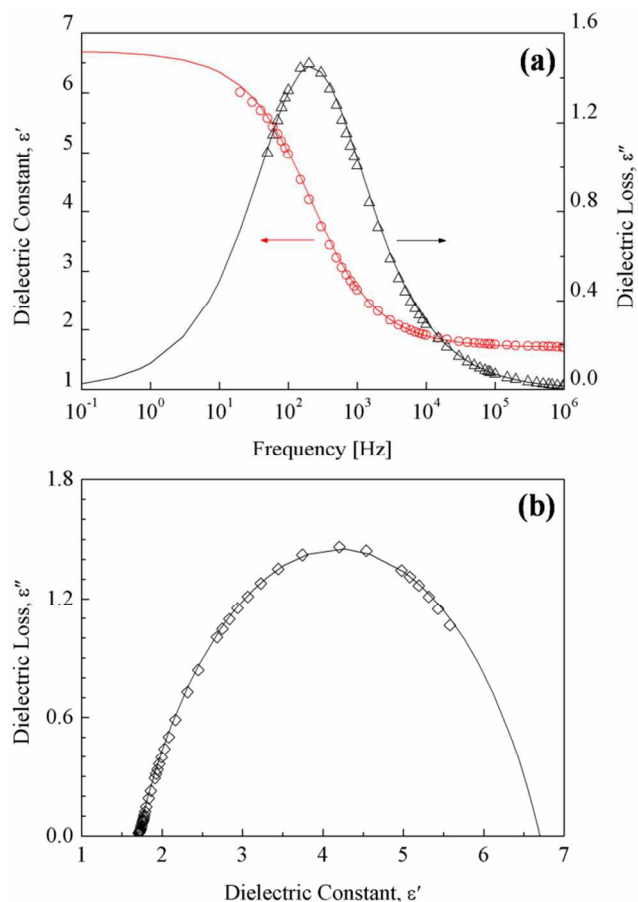


Fig. 9 Relaxation modulus  $G(t)$  of the PANI nanotube-based ER fluid (10 vol%, 50 cS silicone oil) as calculated from  $G'(\omega)$  and  $G''(\omega)$ .

The dielectric properties were examined to verify the ER performance of the PANI nanotube suspension. Fig. 10 shows the dielectric spectra as a function of the frequency, and Cole-Cole fitting plot for the PANI nanotubes-based ER fluid analyzed by the Cole-Cole equation:<sup>53</sup>

$$\epsilon^* = \epsilon' + i\epsilon'' = \epsilon_\infty + \frac{\epsilon_0 - \epsilon_\infty}{(1 + i\omega\lambda)^{1-\alpha}} \quad (5)$$

where  $\epsilon_0$  is the dielectric constant ( $\epsilon'$ ) when the angular frequency ( $\omega$ ) is close to 0 and  $\epsilon_\infty$  is  $\epsilon'$  at the high frequency limit. The difference in the dielectric strength  $\Delta\epsilon = \epsilon_0 - \epsilon_\infty$  indicates the polarizability of the ER fluids and it is correlated with the electrostatic interaction among the particles. The polarizability is generated either from dielectric or conductive mismatch between the carrier medium and dispersed particles considering the dominant factor in the ER effect.<sup>54</sup> The exponent  $(1 - \alpha)$  characterizes the distribution of the relaxation times over the entire frequency range. If  $\alpha = 0$ , equation (5) reduces to the Debye single relaxation time model. The relaxation time ( $\lambda = 1/2\pi f_{\max}$ ) reflects the rate of interfacial polarization when an electric field is applied, where  $f_{\max}$  is the maximum dielectric loss ( $\epsilon''$ ) of an ER fluid. In some studies,  $\epsilon'$  and  $\epsilon''$  have an important role in the ER behavior.<sup>3,55</sup> Therefore, a high dielectric constant has a positive influence on the ER effects. According to the parameters fitted by equation (5),  $\epsilon_0$  and  $\epsilon_\infty$  are 6.7 and 1.7, respectively, and  $\alpha$  is 0.33. The PANI nanotube suspension has a large  $\Delta\epsilon$  over the frequency range,  $10^2$  to  $10^5$  Hz, which shows that it is a good ER fluid<sup>56</sup> with a high dielectric loss peak around  $10^2$  Hz. In addition, the relaxation time ( $\lambda = 0.75$  ms) was very short. A short relaxation time has the feature of fast interfacial polarization, which is related to the faster chain reformation under an applied electric field once the chain has been broken in a higher shear flow field. A short relaxation time corresponds to higher shear stress.<sup>57</sup>



**Fig. 10** (a) Dielectric constant and loss factor as a function of the frequency and (b) Cole-Cole plot of PANI nanotube-based ER fluid (10 vol%, 50 cS silicone oil). The lines were fitted from equation (5).

#### 4. Conclusions

This study examined rheological properties of a PANI nanotube suspension. SEM, TEM, XRD, and BET analysis confirmed the formation of a tubular structure by the micelle soft-template method. The flow responses of the PANI nanotubes-based ER fluid as a function of the shear rate in different electric field strengths were measured. The fluid exhibited considerably higher ER performance because of the higher aspect ratio and strong fibrillation. The dynamic yield stress was also reanalyzed as a function of the electric field indicating a slope of 1.5. In addition, the sensitivity and stability of the ER fluid in an electric field with a square voltage pulse were determined, and the dynamic measurements showed that it exhibited solid like behavior. Furthermore, the dielectric spectra and Cole-Cole plot showed that the polarizability and relaxation time of the ER fluid corresponded well with the ER performance.

#### Acknowledgements

This study was supported by Inha University, Korea.

#### Notes and references

Department of Polymer Science and Engineering, Inha University, Incheon, 402-751, Korea. E-mail: hjchoi@inha.ac.kr

- 1 (a) A.G. MacDiarmid, *Angewan. Chem. Int. Ed.*, 2001, **40**, 2581; (b) Z. Tian, H. Yu, L. Wang, M. Saleem, F. Ren, P. Ren, Y. Chen, R. Sun, Y. Sun and L. Huang, *RSC Adv.*, 2014, **4**, 28195
- 30 2 (a) O. Quatrat and J. Stejskal, *J. Ind. Eng. Chem.*, 2006, **12**, 352; (b) W. Shen, H. Deng and Z. Gao, *RSC Adv.*, 2014, **4**, 53257
- 3 A. Lengálová, V. Pavlínek, P. Sába, O. Quatrat, T. Kitano and J. Stejskal, *Eur. Polym. J.*, 2003, **39**, 641
- 4 Q. Cheng, V. Pavlínek, Y. He, C. Li and P. Saha, *Colloid Polym. Sci.*, 2009, **287**, 435
- 35 5 (a) Y. Yin, C. Liu, B. Wang, S. Yu and K. Chen, *Dalton Trans.*, 2013, **42**, 7233; (b) B. Wang, C. Liu, Y. Yin, S. Yu, K. Chen, P. Liu and B. Liang, *Compos. Sci. Tech.*, 2013, **86**, 89; (c) X. Song, K. Song, S. Ding, Y. Chen and Y. Lin, *J. Ind. Eng. Chem.*, 2013, **19**, 416.
- 40 6 (a) Y.P. Seo and Y. Seo, *Langmuir*, 2012, **28**, 3077; (b) S. Kim, C. Kim, J.Y. Hong, S.H. Hwang and J. Jang, *RSC Adv.*, 2014, **4**, 6821; (c) J. Jiang, Y. Tian and Y. Meng, *Langmuir*, 2011, **27**, 5814
- 7 (a) J.A. Marins, B.G. Soares, A.A. Silva and S. Livi, *RSC Adv.*, 2014, **4**, 50925; (b) J. Wu, T. Jin, F. Liu, J. Guo, Y. Cheng and G. Xu, *RSC Adv.*, 2014, **4**, 29622; (c) W.L. Zhang and H.J. Choi, *Soft Matter*, 2014, **10**, 6601; (d) S.Y. Oh and T.J. Kang, *Soft Matter*, 2014, **10**, 3726
- 8 Y.M. Han, S.C. Lim, H.G. Lee, S.B. Choi and H.J. Choi, *Mater. Des.*, 2003, **24**, 53
- 50 9 J. Furusho, M. Sakaguchi, N. Takesue and K. Koyanagi, *J. Intell. Mater. Syst. Struct.*, 2002, **13**, 425
- 10 K.P. Tan, A.R. Johnson, R. Stanway and W.A. Bullough, *Mech. Machine Theory*, 2007, **42**, 1547
- 11 J. Yin, X. Zhao, L. Xiang, X. Xia and Z. Zhang, *Soft Matter*, 2009, **5**, 4687
- 55 12 (a) J. Lu and X. Zhao, *J. Mater. Chem.*, 2002, **12**, 2603; (b) O. Erol, M. Karakisla, H.I. Unal and M. Sacak, *J. Compos. Mater.*, 2011, **46**, 1295
- 13 J.H. Hwang and S.C. Yang, *Synth. Met.*, 1989, **29**, 271
- 60 14 (a) J.A. Marins, F. Giulieri, B.G. Soares and G. Bossis, *Synth. Met.*, 2013, **185**, 9; (b) J. Yin, X. Zhao, X. Xia, L. Xiang and Y. Qiao, *Polymer*, 2008, **49**, 4413
- 15 J. Yin and X. Zhao, *Nanoscale Res. Lett.*, 2011, **6**, 256
- 16 (a) R.C. Kanu and M.T. Shaw, *J. Rheol.*, 1988, **42**, 657; (b) I. Bica, Y.D. Liu and H.J. Choi, *J. Ind. Eng. Chem.*, 2013, **19**, 394
- 65 17 (a) M.T. Lopez-Lopez, P. Kuzhir and G. Bossis, *J. Rheol.*, 2009, **53**, 115; (b) S.W. Ko, M.S. Yang and H.J. Choi, *Mater. Lett.*, 2009, **63**, 861
- 18 R.C. Bell, J.O. Karli, A.N. Vavreck, D.T. Zimmerman, G.T. Ngatu and N.M. Wereley, *Smart Mater. Struct.*, 2008, **17**, 015028
- 70 19 B.M. Lee, J.E. Kim, F.F. Fang, H.J. Choi and J. Feller, *Macromol. Chem. Phys.*, 2011, **212**, 2300
- 20 J. Yin, X. Xia, L. Xiang, Y. Qiao and X. Zhao, *Smart Mater. Struct.*, 2009, **18**, 095007
- 75 21 J. Yin, X. Xia, L. Xiang, and X. Zhao, *Carbon*, 2010, **48**, 2958
- 22 J. Hong, M. Choi, C. Kim and J. Jang, *J. Colloid Interf. Sci.*, 2010, **347**, 177
- 23 L. Zhang, Y. Long, Z. Chen and M. Wan, *Adv. Funct. Mater.*, 2004, **14**, 693
- 80 24 Z. Zhang, M. Wan and Y. Wei, *Adv. Funct. Mater.*, 2006, **16**, 1100
- 25 H. Ding, J. Shen, M. Wan and Z. Chen, *Macromol. Chem. Phys.*, 2008, **209**, 864
- 26 C. Laslau, Z.D. Zujovic, L. Zhang, G.A. Bowmaker and J. Travas-Sejdic, *Chem. Mater.*, 2009, **21**, 954
- 85 27 Z. Zhang and M. Wan, *Synth. Met.*, 2003, **132**, 205
- 28 M.V. Kulkarni, A.K. Viswanath, R. Marimuthu and T. Seth, *J. Polym. Sci. A: Polym. Chem.*, 2004, **42**, 2043
- 29 S. Wu, F. Zeng and J. Shen, *Polym. J.*, 1998, **30**, 451
- 30 Z. Zhang, Z. Wei and M. Wan, *Macromolecules*, 2002, **35**, 5937
- 90 31 J.P. Pouget, M.E. Jozefowicz, A.J. Epstein, X. Tang and A.G. MacDiarmid, *Macromolecules*, 1991, **24**, 779
- 32 J. Laska, D. Djurado and W. Łuzny, *Eur. Polym. J.*, 2002, **38**, 947
- 33 K. Oz, M. Yavuz, H. Yilmaz, H. Unal and B. Sari, *J. Mater. Sci.*, 2008, **43**, 1451
- 95 34 F.F. Fang, J.H. Kim, H.J. Choi and C.A. Kim, *Colloid Polym. Sci.*, 2009, **287**, 745

- 35 M.S. Cho, Y.H. Cho, H.J. Choi and M.S. Jhon, *Langmuir*, 2003, **19**, 5875
- 36 M. Stenicka, V. Pavlinek, P. Saha, N. Blinova, J. Stejskal and O. Quadrat, *Colloid Polym. Sci.*, 2009, **287**, 403
- 37 C. Lin and J.W. Shan, *Phys. Fluids*, 2007, **19**, art no. 121702
- 38 J.E. Martin, J. Odinek, T.C. Halsey and R. Kamien, *Phys. Rev. E.*, 1998, **57**, 756
- 39 T.M. Kwon, M.S. Jhon and H.J. Choi, *J. Molecular Liq.*, 1998, **75**, 115
- 40 M.S. Cho, H.J. Choi and M.S. Jhon, *Polymer*, 2005, **46**, 11484
- 41 J. Zhu, S. Wei, J. Ryu, M. Budhathoki, G. Liang and Z. Guo, *J. Mater. Chem.*, 2010, **20**, 4937
- 42 D.J. Klingenberg, F. van Swol and C.F. Zukoski, *J. Chem. Phys.*, 1991, **94**, 6170
- 43 R. Stanway, J.L. Sproston, and A.K. El-Wahed, *Smart Mater. Struct.*, 1996, **5**, 464
- 44 (a) M. Sedlacik, M. Mrlík, V. Pavlinek, P. Saha, O. Quadrat, *Colloid Polym. Sci.*, 2012, **290**, 41; (b) W.L. Zhang, H.P. Shang, H.J. Choi, *J. Colloid Interf. Sci.*, 2013, **402**, 100; (c) W.L. Zhang, Y.D. Liu, H.J. Choi, Y. Seo, *RSC Adv.*, 2013, **3**, 11723
- 45 X. Pan and G.H. McKinley, *Appl. Phys. Lett.*, 1997, **71**, 333
- 46 B.D. Chin and H.H. Winter, *Rheol. Acta*, 2002, **41**, 265
- 47 M. Yang, L.E. Scriven and C.W. Macosko, *J. Rheol.*, 1986, **30**, 1015
- 48 (a) J. de Vincente, F. Gonzalez-Caballero, G. Bossis, O. Volkova, *J. Rheol.*, 2002, **46**, 1295; (b) H.M. Laun, C. Gabriel, Ch. Kieburg, *J. Int. Mat. Sys. Struct.*, 2010, **21**, 1479
- 49 J. Hwang, K. Shin, H. Lim, J. Cho, J. Kim and K. Suh, *Macromol. Res.*, 2012, **20**, 391
- 50 B.J. Park, B.O. Park, B.H. Ryu, Y.M. Choi, K.S. Kwon and H.J. Choi, *J. Appl. Phys.*, 2010, **108**
- 51 F.R. Schwarzl, *Rheol. Acta*, 1975, **14**, 581
- 52 R. Prasad, V. Pasanovic-Zujo, R.K. Gupta, F. Cser and S.N. Bhattacharya, *Polym. Eng. Sci.*, 2004, **44**, 1220
- 53 H.J. Choi, C.H. Hong and M. Jhon, *Int. J. Mod. Phys. B*, 2007, **21**, 4974
- 54 Y.C. Lan, S.Q. Men, X.Y. Xu and K.Q. Lu, *J. Phys. D*, 2000, **33**, 1239
- 55 T. Hao, Z. Xu and Y. Xu, *J. Colloid Interf. Sci.*, 1997, **190**, 334
- 56 K. Di, Y. Zhu, X. Yang and C. Li, *Colloids Surf. A: Physicochem. Eng. Aspects*, 2006, **280**, 71
- 57 J.H. Sung, I. Lee, H.J. Choi and S.B. Choi, *Int. J. Mod. Phys. B*, 2005, **19**, 1128